

Sensitivity engineering in direct contact palladium-gold nano-sandwich hydrogen sensors [Invited]

Nikolai Strohfeldt,^{*} Jun Zhao, Andreas Tittl and Harald Giessen

4th Physics Institute and Research Center SCoPE, University of Stuttgart, D-70569 Stuttgart, Germany

^{*}n.strohfeldt@pi4.uni-stuttgart.de

Abstract: In recent years, plasmonic hydrogen sensing schemes using complex hybrid Pd@Au nanostructures have attracted significant attention. However, so far, most studies have focused on investigating the sensing performance of nanosensor geometries where the constituent materials are laterally coupled. In contrast to such planar hybrid systems, which often require complex multi-step fabrication approaches, sensing devices where the materials are stacked directly on top of each other can be fabricated in a single lithography step, enabling straightforward high-throughput processing. Here, we demonstrate a novel hydrogen sensing scheme which incorporates complex hybrid plasmonic nanostructures consisting of stacked gold and palladium nanodisks. In particular, we study the influence of stacking order and geometry, experimentally and numerically, to find an optimal arrangement for a hydrogen sensor device. With an optimized sensing geometry – a stack of gold as lower and palladium as upper disk – we obtain spectral shifts as large as 30 nm at 4 vol.% H₂, which is a strong improvement compared to previous indirect sensing designs. Our samples yield large absorption and scattering signals and are fabricated by low-cost hole-mask colloidal lithography and therefore yield sample sizes over areas of 1 cm².

©2015 Optical Society of America

OCIS codes: (130.6010) Sensors; (160.3918) Metamaterials; (160.4236) Nanomaterials; (280.4788) Optical sensing and sensors.

References and links

1. C. Wadell, S. Syrenova, and C. Langhammer, "Plasmonic hydrogen sensing with nanostructured metal hydrides," *ACS Nano* **8**(12), 11925–11940 (2014).
2. A. Tittl, H. Giessen, and N. Liu, "Plasmonic gas and chemical sensing," *Nanophotonics* **3**(3), 157–180 (2014).
3. C. Langhammer, I. Zorić, B. Kasemo, and B. M. Clemens, "Hydrogen storage in Pd nanodisks characterized with a novel nanoplasmonic sensing scheme," *Nano Lett.* **7**(10), 3122–3127 (2007).
4. E. Maeda, S. Mikuriya, K. Endo, I. Yamada, A. Suda, and J.-J. J. Delaunay, "Optical hydrogen detection with periodic subwavelength palladium hole arrays," *Appl. Phys. Lett.* **95**(13), 133504 (2009).
5. A. Tittl, P. Mai, R. Taubert, D. Dregely, N. Liu, and H. Giessen, "Palladium-based plasmonic perfect absorber in the visible and its applications to hydrogen sensing," *Nano Lett.* **11**, 4366–4369 (2011).
6. C. Langhammer, E. M. Larsson, B. Kasemo, and I. Zorić, "Indirect nanoplasmonic sensing: ultrasensitive experimental platform for nanomaterials science and optical nanocalorimetry," *Nano Lett.* **10**(9), 3529–3538 (2010).
7. M. L. Tang, N. Liu, J. A. Dionne, and A. P. Alivisatos, "Observations of shape-dependent hydrogen uptake trajectories from single nanocrystals," *J. Am. Chem. Soc.* **133**(34), 13220–13223 (2011).
8. A. Tittl, X. Yin, H. Giessen, X.-D. Tian, Z.-Q. Tian, C. Kremers, D. N. Chigrin, and N. Liu, "Plasmonic smart dust for probing local chemical reactions," *Nano Lett.* **13**(4), 1816–1821 (2013).
9. N. Li, A. Tittl, S. Yue, H. Giessen, C. Song, B. Ding, and N. Liu, "DNA-assembled bimetallic plasmonic nanosensors," *Light Sci. Appl.* **3**(12), e226 (2014).
10. R. Jiang, F. Qin, Q. Ruan, J. Wang, and C. Jin, "Ultrasensitive plasmonic response of bimetallic Au/Pd nanostructures to hydrogen," *Adv. Funct. Mater.* **24**(46), 7328–7337 (2014).
11. F. Gu, H. Zeng, Y. B. Zhu, Q. Yang, L. K. Ang, and S. Zhuang, "Single-crystal Pd and its alloy nanowires for plasmon propagation and highly sensitive hydrogen detection," *Adv. Opt. Mater.* **2**(2), 189–196 (2014).

12. F. Gu, G. Wu, and H. Zeng, "Hybrid photon-plasmon Mach-Zehnder interferometers for highly sensitive hydrogen sensing," *Nanoscale* **7**(3), 924–929 (2015).
13. M. E. Nasir, W. Dickson, G. A. Wurtz, W. P. Wardley, and A. V. Zayats, "Hydrogen detected by the naked eye: Optical hydrogen gas sensors based on core/shell plasmonic nanorod metamaterials," *Adv. Mater.* **26**(21), 3532–3537 (2014).
14. N. Liu, M. L. Tang, M. Hentschel, H. Giessen, and A. P. Alivisatos, "Nanoantenna-enhanced gas sensing in a single tailored nanofocus," *Nat. Mater.* **10**(8), 631–636 (2011).
15. T. Shegai, P. Johansson, C. Langhammer, and M. Käll, "Directional scattering and hydrogen sensing by bimetallic Pd-Au nanoantennas," *Nano Lett.* **12**(5), 2464–2469 (2012).
16. S. Syrenova, C. Wadell, and C. Langhammer, "Shrinking-hole colloidal lithography: self-aligned nanofabrication of complex plasmonic nanoantennas," *Nano Lett.* **14**(5), 2655–2663 (2014).
17. A. Yang, M. D. Huntington, M. F. Cardinal, S. S. Masango, R. P. Van Duyne, and T. W. Odom, "Hetero-oligomer nanoparticle arrays for plasmon-enhanced hydrogen sensing," *ACS Nano* **8**(8), 7639–7647 (2014).
18. C. Wadell, T. J. Antosiewicz, and C. Langhammer, "Optical absorption engineering in stacked plasmonic Au-SiO₂-Pd nanoantennas," *Nano Lett.* **12**(9), 4784–4790 (2012).
19. T. J. Antosiewicz, S. P. Apell, C. Wadell, and C. Langhammer, "Absorption enhancement in lossy transition metal elements of plasmonic nanosandwiches," *J. Phys. Chem. C* **116**(38), 20522 (2012).
20. T. Shegai and C. Langhammer, "Hydride formation in single palladium and magnesium nanoparticles studied by nanoplasmonic dark-field scattering spectroscopy," *Adv. Mater.* **23**(38), 4409–4414 (2011).
21. K. Ikeda, S. Uchiyama, M. Takase, and K. Murakoshi, "Hydrogen-induced tuning of plasmon resonance in palladium–silver layered nanodimer arrays," *ACS Photonics* **2**(1), 66–72 (2015).
22. S. Cataldo, J. Zhao, F. Neubrech, B. Frank, C. Zhang, P. V. Braun, and H. Giessen, "Hole-mask colloidal nanolithography for large-area low-cost metamaterials and antenna-assisted surface-enhanced infrared absorption substrates," *ACS Nano* **6**(1), 979–985 (2012).
23. J. Zhao, B. Frank, F. Neubrech, C. Zhang, P. V. Braun, and H. Giessen, "Hole-mask colloidal nanolithography combined with tilted-angle-rotation evaporation: A versatile method for fabrication of low-cost and large-area complex plasmonic nanostructures and metamaterials," *Beilstein J. Nanotechnol.* **5**, 577–586 (2014).
24. A. Tittl, M. G. Harats, R. Walter, X. Yin, M. Schäferling, N. Liu, R. Rapaport, and H. Giessen, "Quantitative angle-resolved small-spot reflectance measurements on plasmonic perfect absorbers: impedance matching and disorder effects," *ACS Nano* **8**(10), 10885–10892 (2014).
25. R. W. Wood, "XLII. On a remarkable case of uneven distribution of light in a diffraction grating spectrum," *Philos. Mag. Ser. 6* **4**(21), 396–402 (1902).
26. P. B. Johnson and R. W. Christy, "Optical constants of the noble metals," *Phys. Rev. B* **6**(12), 4370–4379 (1972).
27. K. von Rottkay, M. Rubin, and P. A. Duine, "Refractive index changes of Pd-coated magnesium lanthanide switchable mirrors upon hydrogen insertion," *J. Appl. Phys.* **85**(1), 408 (1999).
28. A. B. Dahlin, J. O. Tegenfeldt, and F. Höök, "Improving the instrumental resolution of sensors based on localized surface plasmon resonance," *Anal. Chem.* **78**(13), 4416–4423 (2006).
29. N. Strohhfeldt, A. Tittl, and H. Giessen, "Long-term stability of capped and buffered palladium-nickel thin films and nanostructures for plasmonic hydrogen sensing applications," *Opt. Mater. Express* **3**(2), 194 (2013).
30. A. Baldi, T. C. Narayan, A. L. Koh, and J. A. Dionne, "In situ detection of hydrogen-induced phase transitions in individual palladium nanocrystals," *Nat. Mater.* **13**(12), 1143–1148 (2014).
31. R. Bardhan, L. O. Hedges, C. L. Pint, A. Javey, S. Whitelam, and J. J. Urban, "Uncovering the intrinsic size dependence of hydriding phase transformations in nanocrystals," *Nat. Mater.* **12**(10), 905–912 (2013).
32. C. Wadell, T. Pingel, E. Olsson, I. Zorić, V. P. Zhdanov, and C. Langhammer, "Thermodynamics of hydride formation and decomposition in supported sub-10nm Pd nanoparticles of different sizes," *Chem. Phys. Lett.* **603**, 75–81 (2014).
33. K. M. Mayer and J. H. Hafner, "Localized surface plasmon resonance sensors," *Chem. Rev.* **111**(6), 3828–3857 (2011).
34. T. Hübert, L. Boon-Brett, G. Black, and U. Banach, "Hydrogen sensors - A review," *Sens. Actuators B Chem.* **157**(2), 329–352 (2011).

1. Introduction

Over the last decade, the concept of a hydrogen economy has emerged as a topical and highly debated candidate for replacing fossil fuels in large-scale energy production. However, this important development is still hampered by a lack of cheap, reliable, safe and compact hydrogen sensors that can be used for monitoring all process steps of the hydrogen production and consumption chain, from energy plants to hydrogen-fueled cars.

To this end, a variety of possible sensing concepts have been proposed and evaluated [1,2]. Initial experiments focused mainly on plasmonic structures with large nanostructured areas, by employing geometries such as nanodisks, hole arrays, and perfect absorbers [3–5]. Moving from extended systems towards progressively lower detection volumes, single

particle nanosensor geometries, such as nanostructured antennas [6] and chemically synthesized “smart dust” nanoprobos [7–10], were investigated. One important concept for high sensitivity palladium-based plasmonic hydrogen sensors is the integration of multiple materials into a single hybrid nanosensor geometry. Here, gold or silver nanostructures are commonly used to enhance the changes in other chemically reactive materials, since they yield the highest field enhancement and the narrowest plasmonic resonances in the visible and near-infrared wavelength region. There are some concepts involving alloyed nanostructures [11,12] and also core-shell pillars forming a metasurface [13] that are used as plasmonic hydrogen detectors. However, most hybrid hydrogen sensing geometries investigated so far involve the lateral placement of palladium and gold antennas with surface-to-surface distances around 10nm [14–16], the placement of gold and palladium disks on the sides of a nanopyramide [17], or the stacking of a palladium disk on top of a gold antenna with a dielectric spacer in between [18–20].

In all these geometries, one key unifying design goal is to place the two constituent materials at very close surface-to-surface distances while preventing direct contact. This is usually achieved either by complex two-layer lithography steps [14] or by introducing a spacer layer between the two materials [6]. In many earlier approaches, direct contact between the noble metal used for the antenna and the highly reactive but often strongly damped functional material, is assumed to be detrimental for the sensitivity of the full structure. Therefore, only very recently palladium on top of silver triangles have been studied in comparison to palladium-silver heterodimers [21].

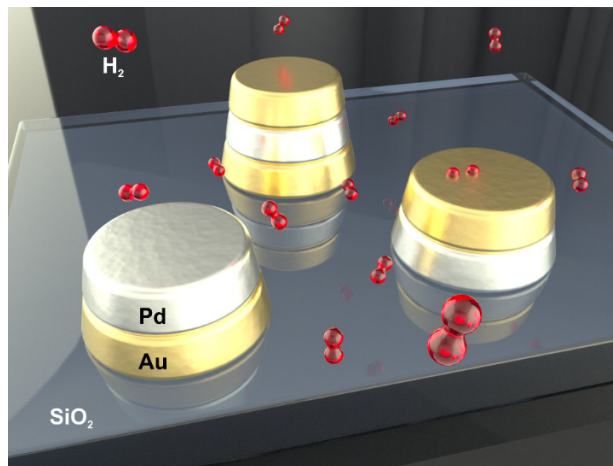


Fig. 1. Schematic view of the different palladium-gold nanodisk systems under investigation. The stacking sequence of gold and palladium is varied.

Here, we investigate the sensing performance of hybrid plasmonic nanosensor geometries consisting of stacked gold and palladium nanodisks in direct contact. We employ colloidal hole-mask lithography to fabricate the nanostacks [22], and perform hydrogen-dependent time-resolved transmittance measurements to investigate geometries with different material placement and number of constituent disks. Especially, we find that the order of materials in the nanostacks plays a crucial role for both the sensitivity and the response time of the structures.

The resulting insight should ease the way to fabricate reliable, highly sensitive, low-cost hydrogen sensors with good temporal response that are ideally suited for technological applications.

2. Results and Discussion

To conduct a thorough study on direct contact palladium gold nanodisk stacks, we investigate three alternating vertical arrangements of two or three nanodisks. Figure 1 shows a schematic view of the investigated designs. Each geometry was experimentally realized using hole-mask colloidal lithography, which produces disk stacks with high density, random placement and large-area coverage [23]. Therefore, this method is ideally suited for studying the plasmonic effects of such nanodisk stacks without the disturbance of grating effects [24] such as the Wood-anomaly [25]. An additional advantage of hole-mask colloidal lithography is the absence of any residual dielectric resist (PMMA) from the fabrication process in contact with the disks.

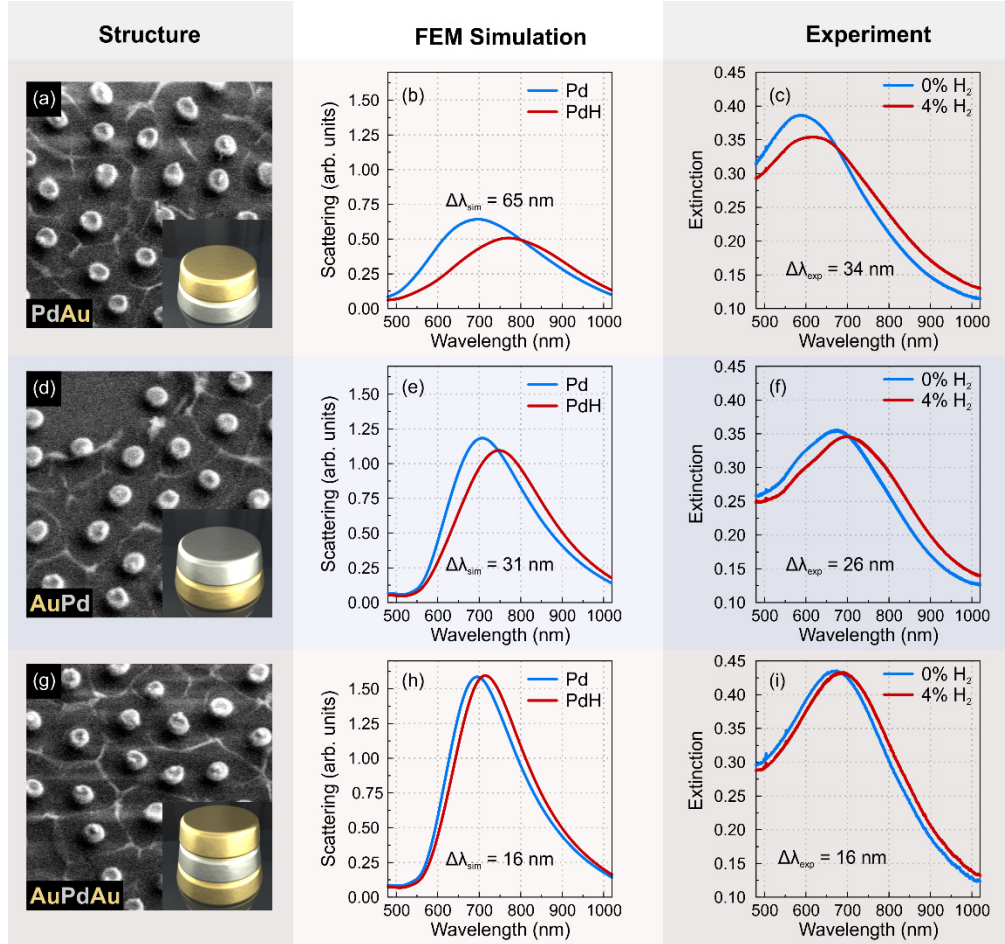


Fig. 2. Simulated and measured spectra of the nano-sandwich structures with (red curves) and without hydrogen (blue curves). (a) Exemplary SEM image of the Pd-Au system. (b) Single particle scattering FEM simulation of the Pd-Au system using tabulated Pd and PdH data. The spectra display a redshift and broadening when going from Pd to PdH. (c) Extinction measurements of the fabricated system showing the same qualitative behavior as the simulations. (d) – (i) SEM images, simulation and measurement data for the other two sandwich systems.

Samples with different stacking geometries are characterized with a scanning electron microscope (SEM) as shown in the left column in Fig. 2, together with schematic views of the respective structures. All the Pd and Au disks have the same basic geometry, with a diameter

of about 150 nm (lowest disk) and a thickness of about 20 nm. The cobweb-like structures around the disks in the SEM images arise from very small amounts of residual PMMA left over from the fabrication process. Still, the PMMA is sufficiently separated from the disk stacks to have no significant influence on their optical properties.

In the center column of Fig. 2, we show single particle scattering FEM simulations of the studied structures using tabulated constants for Au, Pd (blue curves) and PdH (red curves) [26,27]. All systems exhibit a redshift and broadening of the plasmonic resonance when using PdH dielectric data compared to Pd. The ensemble extinction spectra of three fabricated large-area samples, which are measured in pure nitrogen atmosphere (blue curves) and with 4 vol.% hydrogen in nitrogen carrier gas (red curves) using a white light transmission spectroscopy system, are shown in the right column in Fig. 2. The experimental results agree very well with the simulations, both considering the resonance width and position as well as the hydrogen sensing performance, which manifests as a red-shift and broadening of the plasmonic resonance upon hydrogen exposure.

However, there are some visible differences between experiment and simulation. Particularly, in the case of the Pd-Au nanostack, the fabricated structures exhibit a plasmonic resonance at lower wavelengths when compared to the simulated structures. This can mostly be attributed to material defects or fabrication tolerances, which may result in a smaller gold disk in the second layer, compared to the design in simulation (due to the clogging effect from the hole-masks). However, the size difference is challenging to determine, since SEM measurements cannot distinguish between palladium and gold, and element-resolved TEM methods cannot be easily applied to samples fabricated using hole-mask colloidal lithography.

The difference between the measured and numerically predicted resonance shifts in the Pd-Au system can be attributed in part to material defects and palladium-gold alloying, which are more significant when the palladium is placed below the gold disk. Nevertheless, apart from the resonance shift, all other properties such as the predicted hydrogen-induced changes in resonance amplitude and width are well reproduced in the experiment.

Focusing now on the hydrogen sensing performance of our nanostack geometries, we find a clear difference between the first (Pd-Au) and the remaining two systems (Au-Pd, Au-Pd-Au).

The Pd-Au stack shows a relatively broad resonance which is blue-shifted compared to the other systems. However, the resonance change upon hydrogen exposure is relatively large (65nm in simulation and about 34nm in experiment). Thus, this system can be considered palladium-like, due to the strong influence of the palladium disk on the overall plasmon resonance.

The second category systems (Au-Pd, Au-Pd-Au) exhibit a relatively narrow resonance more similar to the one of a sole gold disk. Upon hydrogen exposure there is a resonance red-shift with a relatively small decrease in resonance amplitude. Thus, in contrast to the Pd-like stack, the gold disk is the main driver of the plasmonic resonance, rendering the whole system more gold-like. This becomes obvious when considering that the Au-Pd-Au system (which includes two gold disks, coupled through the palladium disk) exhibits the narrowest resonance with virtually no change in resonance amplitude upon H₂ exposure.

Synopsizing, the Au-Pd-Au system shows the strongest and narrowest resonance with a full width at half maximum (FWHM) of approx. 210 nm, but only a small wavelength shift of 16 nm upon hydrogenation. The Au-Pd stack with a somewhat larger FWHM of about 235 nm in the unhydrogenated state and 255 nm as Au-PdH, however, exhibits twice the hydrogen-induced wavelength shift of almost 30 nm. For the Pd-Au system we have a significantly larger resonance width, with a FWHM of about 310 nm. Nevertheless, in exchange, the system yields larger wavelength shifts upon hydrogenation.

To evaluate the performance of a plasmonic geometry for hydrogen sensing applications, it is not only important to look at the final optical response at various hydrogen concentrations, but also to study the temporal behavior of such a device. For example in the

context of industrial hydrogen sensing, detector geometries with a large optical change upon hydrogen exposure are only useful if the change also happens on a reasonable timescale. Therefore, we have also investigated the hydrogen loading and unloading dynamics for various concentrations in all previously discussed stacking geometries.

In the experiments, ensemble extinction spectra were recorded every 5 seconds while the samples were exposed to sequences of different hydrogen concentrations in nitrogen carrier gas at a constant gas flow-rate of 1 l/min. The concentration sequence starts with 200 sec of 0.5 vol.% H₂ in N₂, followed by 200 sec of pure nitrogen, then 200 sec at 1 vol.% H₂ and so on, until a maximum H₂ concentration of 5 vol.% is reached. Figure 3 shows the resulting time-dynamics of the plasmon-peak wavelength for the three geometries exposed to such a hydrogen sequence. The plasmon peak positions for the different stacks (exemplarily shown for the Au-Pd stack in Fig. 3(a)) are obtained by employing a centroid method that calculates the center of mass of the extinction peak. This method offers a very robust and reliable way of detecting even small peak-shifts independent of the peak shape and noise in the spectral data [8,28]. As already mentioned, the two-layer stack with gold as a lower disk gives a strong shift of about 30 nm. However, this geometry not only exhibits a large plasmon resonance shift, but also shows the fastest loading and unloading behavior with about 50 sec to reach the maximum response for 5% H₂ (see Fig. 3(a) and green lines in Fig. 3(b) and 3(c)).

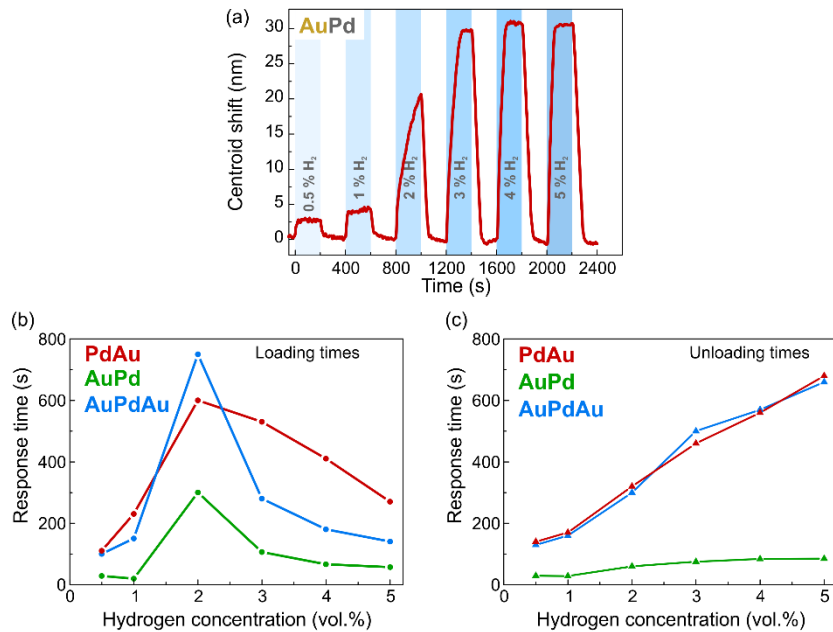


Fig. 3. (a) Exemplary time trace of the centroid wavelength shifts upon a sequence of hydrogen gas exposure, going from 0.5 – 5 vol.% hydrogen in nitrogen for the Au-Pd system. (b) Extracted loading times for different hydrogen concentrations for all three sensing geometries. Note, the exceptionally high loading time for 2 vol.% H₂ observed in all systems is related to a phase transition from α - to β -phase in Pd. (c) Extracted unloading times for the same concentration steps as in (b) for all three sensing geometries. All systems show a distinct reaction to the different hydrogen concentrations, where the Au-Pd system performs the fastest in both loading and unloading times (<100s, except at 2 vol.%).

The other two geometries with the palladium disk placed below the gold disk (Pd-Au, Au-Pd-Au) both show dramatically longer loading and unloading times (blue and red lines in Fig. 3(b) and 3(c)). At 5 vol.% H₂, for example, unloading times above 200 sec are observed for both cases as well as loading times of about 100 sec (Au-Pd-Au) and even above 200 sec for the Pd-Au case. Since all samples were measured directly after fabrication and manufactured

using the same materials and under the same conditions, the strong differences in the temporal behavior cannot be attributed to material differences or sample degradation [29].

Since the open surface area of the palladium plays a crucial role for both the loading and unloading process, it is easy to understand that the geometry with the palladium disk on top and hence the highest relative open surface area, exhibits the fastest hydrogen ab- and desorption processes. In the other two systems, the Pd disk is effectively buried between a gold disk and either another disk or the substrate. Therefore, only the sidewalls of the disks provide the needed catalytic surface for splitting and absorbing of hydrogen molecules or in case of unloading the available surface area for hydrogen recombination. This leads to a strong increase in both loading and unloading times, since all hydrogen ions have to ab- and desorb through the bottleneck of the sidewalls. However, concerning loading times, the three-disk Au-Pd-Au stack is still reacting slightly faster than the Pd-Au system. This might be due to the fabrication process, which leads to strongly decreasing disk diameters for increasing stack heights. Therefore, the third disk is disproportionally smaller than the lower two disks, leading to a higher open surface for the middle disk and this accelerates the reaction process.

All recorded time-traces show that no matter how fast any of the sensors reacts, the maximum centroid shift is only concentration dependent up to a concentration of about 3 vol.% H₂ in N₂ (see Fig. 3(a)). For higher concentrations, only the reaction time changes, but not the shift amplitude. Additionally, the maximum shift per concentration shows a strong jump at about 2 vol.% from less than 5 nm for lower concentration to over 10 nm shift for higher H₂ concentrations, accompanied with a strongly enlarged loading time at 2 vol.% H₂ (see maxima in Fig. 3(b)). This behavior is typical for palladium nanostructures and is related to the occurrence of a phase transition between the so-called α and β -phases in palladium, where H is either interstitial (α -Phase) or build in as PdH (β -Phase). For bulk palladium this phase transition sets in at about 1 to 2 vol.% hydrogen at room temperature and ambient pressures, leading to a saturation behavior for higher concentrations. However, in nanostructured Pd the transition pressure is increased to higher concentrations [30–32]. To avoid the saturation effect in sensing applications at high partial hydrogen pressures, palladium can be alloyed with other metals such as Au, Ni, or Ag [29].

The time-resolved measurements in Fig. 3 clearly show that it is not only important to study the maximum optical response of any nanoplasmonic sensing scheme, but also take into account the relative “free surface area” of the system, which strongly alters the temporal response of a system.

Depending on the target application, either of the systems has specific advantages. If large wavelength shifts upon hydrogen exposure (hence large sensitivities) are required, Pd-like system such as the Pd-Au stacks are ideally suited. However, if the main focus is on fast reaction times, a system with a large open surface area is advantageous, leading to fast loading and unloading times at the expense of smaller hydrogen-induced spectral shifts.

To further explore the origin of the strong differences in sensing performance for the various stacked hydrogen-sensing geometries, it is instructive to also examine the electric fields and current densities of the respective geometries in addition to the spectral shifts. Due to the challenges associated with mapping plasmonic near-fields experimentally, we concentrate on FEM simulations of our system.

To accurately represent the experimental geometries, we modeled truncated Au and Pd cones with a bottom diameter of 150nm and a tapering angle of about 8.5°. The simulations were performed using the CST Microwave Studio 2014 finite element solver with single structures placed on an infinite SiO₂ substrate. Single particle simulations are required, since ensemble simulations using randomly placed structures are not possible with our simulation tool and any periodic assembly would give rise to grating effects [25].

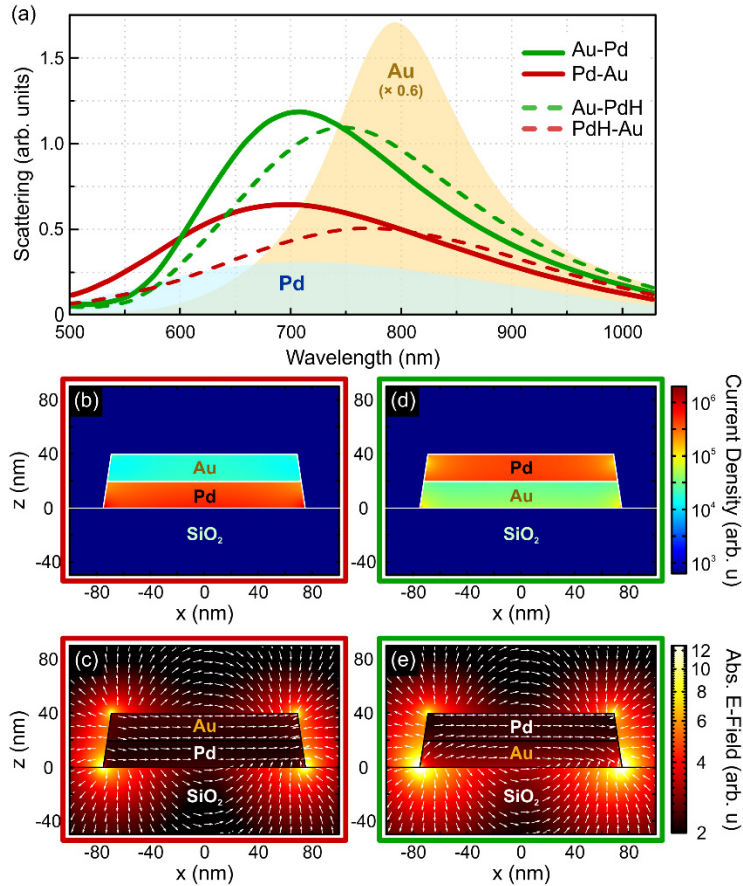


Fig. 4. (a) Calculated single particle scattering spectra for the Au-Pd (green) and Pd-Au system (red) in the hydrogenated (dashed lines) and unhydrogenated states (solid lines). The Au-Pd system exhibits a stronger resonance and is slightly blue-shifted when compared to the Pd-Au system. Nevertheless, both systems show a red-shift and broadening of the resonance when going to the hydrogenated state. Additional spectra for a sole Au (dark yellow shaded) and Pd disk (light blue shaded area) are included for comparison. (b) Calculated current densities for the Pd-Au system at the resonance frequency showing strong optical currents in the palladium nanodisk. (c) Calculated absolute electric fields together with the field vectors for the same geometry and frequency as in (b), depicting the strongest field at the bottom edge of the structure and in-phase oscillations in the Au and Pd disks. (d) and (e) display the current densities and electric fields of the Au-Pd system which exhibit notably enhanced fields and currents in the Au disk, compared to the geometry in (b) and (c).

First, let us have a closer look at the two-disk stacks. The calculated single particle scattering spectra for these two systems are shown in Fig. 4(a) (green and red curves) together with the respective spectra for single Au and Pd disks on SiO₂ (yellow and blue shaded areas). Figure 4, panels b-e show the logarithmically plotted current densities and absolute values for the electric field on a cut-plane through the middle of the structures at the respective resonance frequencies.

When considering the electric fields in the two- and three-disk stack geometries (Figs. 4(c), 4(e) and Fig. 5(b)), we observe a clear dipolar pattern for all systems. Importantly, the electric fields inside the disks are oriented in phase, indicating that the sandwich system can actually be considered as a single plasmonic resonator. This is mainly due to the fact that all disks are in direct conductive contact. Additionally, both the Au and Pd disk exhibit

plasmonic resonances between 600 and 800 nm, resulting in spectral overlap and consequently similar resonant properties (see yellow and blue shaded areas in Fig. 4(a)).

For the Pd-Au structures (red curve in Fig. 4(a) and Figs. 4(b) 4(c)) the plasmon resonance is broadened compared to the Au-Pd system. The reason for this can be understood again by examining the current densities in the metal nanodisks (Fig. 4(b) and 4(d)). Nearly all of the oscillating optical currents are located in the Pd-part of the disk-stack. This is for two reasons, first, palladium has a higher intrinsic damping than gold ($\epsilon_{2_{Pd}} > \epsilon_{2_{Au}}$), which leads to higher Ohmic losses in the material and consequently higher optical currents in the relevant wavelength region ($\sigma_{opt} \propto \epsilon_2$). Therefore, in that spectral region, the palladium structures always exhibit a higher current density than the gold, independent of the geometrical arrangement.

Second, and more relevant for understanding the differences between the two systems in Fig. 4, the palladium disk is in contact with the substrate and hence to a material with a significantly higher refractive index compared to the air surrounding the upper gold disk. For nanostructures, contact to high refractive index materials leads to a concentration of energy close to the interface. This symmetry breaking is also the main reason for the different behavior of the Au-Pd and Pd-Au systems and without the substrate, both systems would essentially give the same field and spectral results.

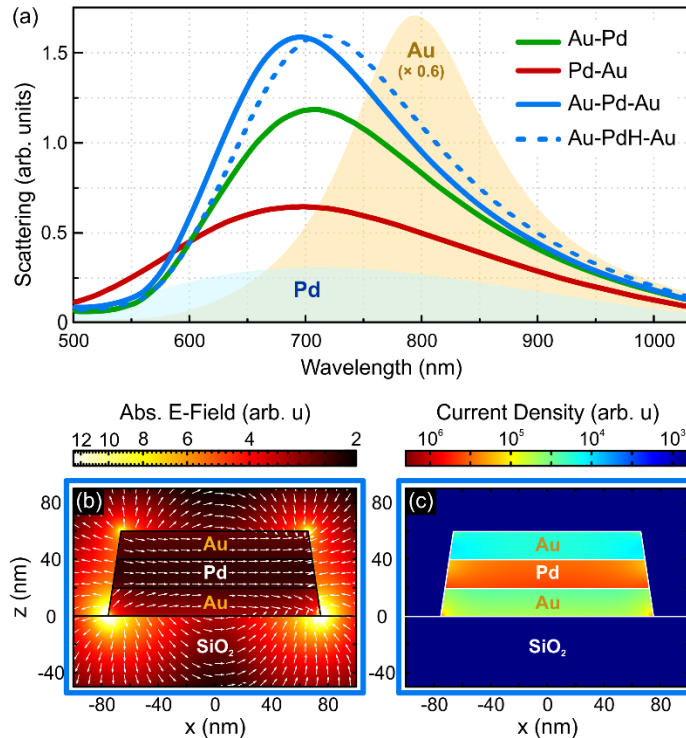


Fig. 5. (a) Calculated single particle scattering spectra of the Au-Pd-Au disk stack in the unhydrogenated (blue solid line) and hydrogenated state (blue dashed line), demonstrating that the structure exhibits a blue-shift and signal increase compared to the respective two disk structure (Au-Pd). The spectra of the two disk stacks and single disks are also plotted (green and red lines) for comparison. (b) Calculated absolute electric fields together with the field vectors for the Au-Pd-Au structure on SiO_2 . The field vectors show that, at resonance, the electric field oscillates in phase in all three disks, resulting in a collective resonance for all the particles. (c) Calculated current densities for the same structure.

Taking into account the substrate effect and the fact that the disk-stack can be treated as one resonator, we find that the collective electron oscillations in the Pd-Au stack lead to a more damped resonance in the blue wavelength region that can be seen as more “palladium-like”. In the Au-Pd case, however, we have a narrower, stronger and red-shifted resonance that can be called more “gold-like”. This is also supported by the stronger electric fields and the higher optical currents in the gold disk when compared to the Pd-Au system (see Fig. 4(b),4(d)).

These insights can be further expanded when moving from the two-disk stacks to the more complex Au-Pd-Au sandwiches displayed in Fig. 5. The two gold antennas enhance the oscillator strength to induce the strongest resonance of all systems, as shown by the unhydrogenated spectra (blue solid line in Fig. 5(a)). The spectra are blue-shifted, with higher scattering amplitude, compared to the Au-Pd two-disk stack (green line). However, the resonances of both systems are still very similar, since the addition of another (gold) disk on top (and therefore farther away from the substrate) has little effect on the fact that the Au-Pd-Au system exhibits a gold-like resonance similar to the Au-Pd stack. This is also supported by the field-plot in Fig. 5(b) and the current densities in Fig. 5(c), showing the collective oscillations of all three disks with strongest fields at the edges of the lowest disk while experiencing the strongest currents in the gold compared to the other two systems in Fig. 4.

The blue-shifted resonance wavelength of the Au-Pd-Au system compared to the Au-Pd stack follows from the fact that the total height of the combined system increases, which leads to a blue-shift of the plasmonic resonance assuming the other dimensions remain constant [33].

Intuitively, an additional gold-disk should produce increased oscillator strength, near-field enhancement, and consequently the largest hydrogen-induced changes. However, the Au-PdH-Au spectra plotted in Fig. 5(a) exhibit the smallest wavelength shifts of all investigated geometries. The reason for this becomes obvious when examining the electric near-fields in Fig. 5(b). In fact, the addition of a top Au disk moves the hotspots of the electric field away from the Pd disk, resulting in lower sensitivity. This is supported by the current densities in the Pd disk (Fig. 5(c)), which are significantly lower than in the two-disk cases.

2. Conclusion

In conclusion, we have studied – theoretically and experimentally – the plasmonic behavior as well as the hydrogen sensing performance of different stacked direct contact palladium and gold nanodisks. Moving towards a different direction in comparison to the majority of indirect sensing schemes in the literature, where direct contact between materials was considered detrimental, we find that the direct-contact palladium-gold disk nanostacks show very good sensing results while easily implemented.

One intriguing aspect of the direct contact scheme is that despite the stacks being comprised of individual gold and palladium nanostructures, they form one collective plasmonic mode. This mode can behave more gold- or palladium-like, depending on the stacking order. Especially, we find that the material directly adjacent to the substrate determines the character of plasmonic response of the complete system. Therefore, if one is looking for the system that shows the best sensitivity while being less demanding concerning the reaction times, it is best to use a palladium-like structure. When, however, the main focus of the application lies on the temporal sensing performance, it is most useful to consider a direct contact scheme with palladium on top, such as the Au-Pd stack we investigated.

Overall the investigations show a promising road towards low-cost, large-area, easy to fabricate direct contact hydrogen sensors. Variations in size and form of the antennas can be considered to further optimize the resonance quality and sensing performance of the systems. Our geometries can also easily be implemented in many of the optical sensing devices that have been developed [29,34], since the nanostructures yield high signal modulation over large areas and have no restrictive demands on the substrate materials.

Acknowledgments

We thank Florian Sterl for help with the analysis of the simulation data. This work was financially supported by the Deutsche Forschungsgemeinschaft (SPP1391, FOR730, GI 269/11-1), the Bundesministerium für Bildung und Forschung (13N9048 and 13N10146), the ERC Advanced Grant COMPLEXPLAS, the Baden-Württemberg Stiftung (Spitzenforschung II), and the Ministerium für Wissenschaft, Forschung und Kunst Baden-Württemberg (Az: 7533-7-11.6-8).